Marine and Petroleum Geology 170 (2024) 107140

Contents lists available at ScienceDirect

Marine and Petroleum Geology

journal homepage: www.elsevier.com/locate/marpetgeo

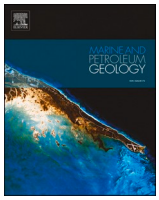

How marine incursions affect the sedimentary environment and the quality of source rocks in the Upper Cretaceous Songliao Basin, NE China

Ruiqian Chen [a,b,*], Xin Bai [c], Chengzheng Huang [a,b], Xia Wu [a,b], Fei Shang [d]

[a] State Key Laboratory of Petroleum Resources and Engineering, China University of Petroleum (Beijing), Beijing, 102249, China
[b] College of Geosciences, China University of Petroleum (Beijing), Beijing, 102249, China
[c] PetroChina Changqing Oilfield Shale Oil Company, Qingyang, 745000, China
[d] Research Institute of Petroleum Exploration & Development, China National Petroleum Corporation, Beijing, 100083, China

ARTICLE INFO

Keywords:
Marine incursion
Qingshankou formation
Lacustrine source rocks
Paleoenvironment

ABSTRACT

The linkage between marine incursions and lacustrine petroleum source rock deposition has been studied worldwide. A variety of interpretations have been suggested to explain the influence of marine incursions on the quality of source rocks in the Upper Cretaceous Qingshankou Formation (K_2qn), Songliao Basin. In this study, high-resolution of geochemical and sedimentary results of two drilled wells from the K_2qn were presented to improve the understanding on this issue. 117 samples from Well GY8HC of the Qijia-Gulong Sag (brief as Gulong Sag) and 251 samples from Well ZY1 of the Sanzhao Sag, the Central Depression of the basin were analyzed to establish the evolution of paleoenvironment and the influence of marine incursions on organic matter enrichment in the two sags. All the evidence suggests that marine incursions have a positive effect on the quality of member 1 of the K_2qn source rocks (K_2qn^1) in the Sanzhao Sag, which was probably due to the rising lake level and increasing salinity of the watermasses. The enhanced salinities could have inhibited lake overturn and oxygenation of bottom water, and thus created a favorable condition for the preservation of organic matter. In contrast, the K_2qn^1 source rock in the Gulong Sag was less affected by marine incursions, which is likely due to the Daqing placanticline blocking two sags. The lake water in the Gulong Sag was characterized as fresh-brackish with less mixing of seawater. Petrographic observation suggests that organic matter in the Gulong source rocks was mainly derived from lacustrine algal and microsporinite. This research provides novel insights into the linkage between marine incursions and the depositional environment during the formation of K_2qn^1 in the Songliao Basin.

1. Introduction

The Songliao Basin stands out as the world's longest surviving super-large lake basin (Wang et al., 2013a, 2013b; Cao et al., 2020). The basin has experienced a greenhouse climate during the Cretaceous and thus could be an excellent site for studying the evolution of paleoclimate and paleoenvironment during this time of period. During the Cretaceous, greenhouse conditions were characterized by the "Three Highs," (i.e., high carbon dioxide concentration, high temperature, and high sea level) (Wang et al., 2024). Over the last sixteen years, the International Continental Scientific Drilling Program (ICDP) has revealed the underlying dynamics of Cretaceous sea-level fluctuations and has confirmed the occurrences of marine incursion events in the Songliao Basin (Wang et al., 2024). Furthermore, the marine incursion events in the Songliao Basin have been studied and supported by the discovery of marine calcareous nannofossils (Huang and Huang, 1998), benthic foraminifera (Xi et al., 2011) and dinoflagellate steranes (Hou et al., 2000) in organic-rich shales in the Qingshankou Formation (K_2qn). Other evidence of marine transgression includes pyrite morphology (Wang et al., 2013a) and associated sulfur geochemistry records (Huang et al., 2013; Cao et al., 2020, 2021). The most recent investigation into dolostones from the member 1 of the Qingshankou Formation (K_2qn^1) introduces a pioneering mineralogical indicator supporting the episodic marine transgressions (Liu et al., 2023).

Many studies have demonstrated that marine incursions have positive effects on the formation of petroleum source rocks in the Upper Cretaceous Qingshankou Formation, which are the dominant source of oil and gas in the Songliao Basin (Zhao et al., 2010; Feng et al., 2011).

* Corresponding author. State Key Laboratory of Petroleum Resources and Engineering, China University of Petroleum (Beijing), Beijing, 102249, China.
E-mail address: richen@cup.edu.cn (R. Chen).

https://doi.org/10.1016/j.marpetgeo.2024.107140
Received 24 August 2024; Received in revised form 26 September 2024; Accepted 27 September 2024
Available online 30 September 2024

These researchers believe that marine incursion from the Western Pacific enter the Songliao paleolake from the southeast, bringing abundant nutrients such as salt and sulfur, resulting in increased primary productivity (Hu et al., 2015; Zhu et al., 2023). Furthermore, the intrusion of high density and high salinity water led to the stratification of the lake water column, which enhanced the reducing environment of the bottom water (Jones et al., 2018; Liu et al., 2023; Zhu et al., 2023). In addition, the biological blooming in the lake basin further intensified the consumption of oxygen and promoted bottom water anoxia, which contributed to large quantities of organic carbon accumulated in the basin during the Qingshankou Formation (Xu et al., 2015; Hou et al., 2022). For example, the organic carbon content (TOC) is highly concentrated during the deposition of the Qingshankou Formation. The TOC content increases basinwards and can be as high as 20% in oil shales at the base of the Qingshankou Formation in most of the Central Depression area (Wang et al., 2013b). However, some researchers consider it challenging to determine the effects of marine incursions on the Qingshankou lacustrine shale (Huang et al., 2013; Wu et al., 2023). They suggested that the degree of marine incursions was not strong in some parts of the basin and thus the preservation of organic matter was controlled by the fluctuation of lake level. Others believe that the evolution of paleo Songliao lake was not only controlled by the global sea level rise but was also influenced by regional tectonics (Zou et al., 2019). Consequently, more research is required to reveal the effects of marine incursions on the depositional environment and the quality of source rock within the Qingshankou Formation.

Previous research has shown that the organic carbon enrichments and the estimated shale oil reserves vary greatly among different sags in the Central Depression of the Songliao Basin. Corresponding to the spatial lithofacies change in the Qingshankou Formation across the Central Depression, the calculated resource estimates for shale oil varied greatly from the Gulong Sag (27.29 billion tons), which located in the west of the Central Depression to the Sanzhao Sag (32.54 billion tons), located in the east of the Central Depression (Sun et al., 2023) (Fig. 1). Therefore, the Central Depression of the basin may provide a suitable geological unit for investigating the influence of marine incursions, and for better resolving its impact on the quality of source rocks.

In this study, the influences of marine incursions on the enrichment of organic carbon in the Central Depression are studied using two drilled wells: the Well GY8HC from the Gulong Sag and the Well ZY1 from the Sanzhao Sag (Fig. 1). This study focuses on high-resolution comparison using trace elements, strontium (Sr) isotope and sedimentary features, to illustrate the temporal and spatial variations of the paleoclimate and paleoenvironment during the deposition of the Qingshankou Formation.

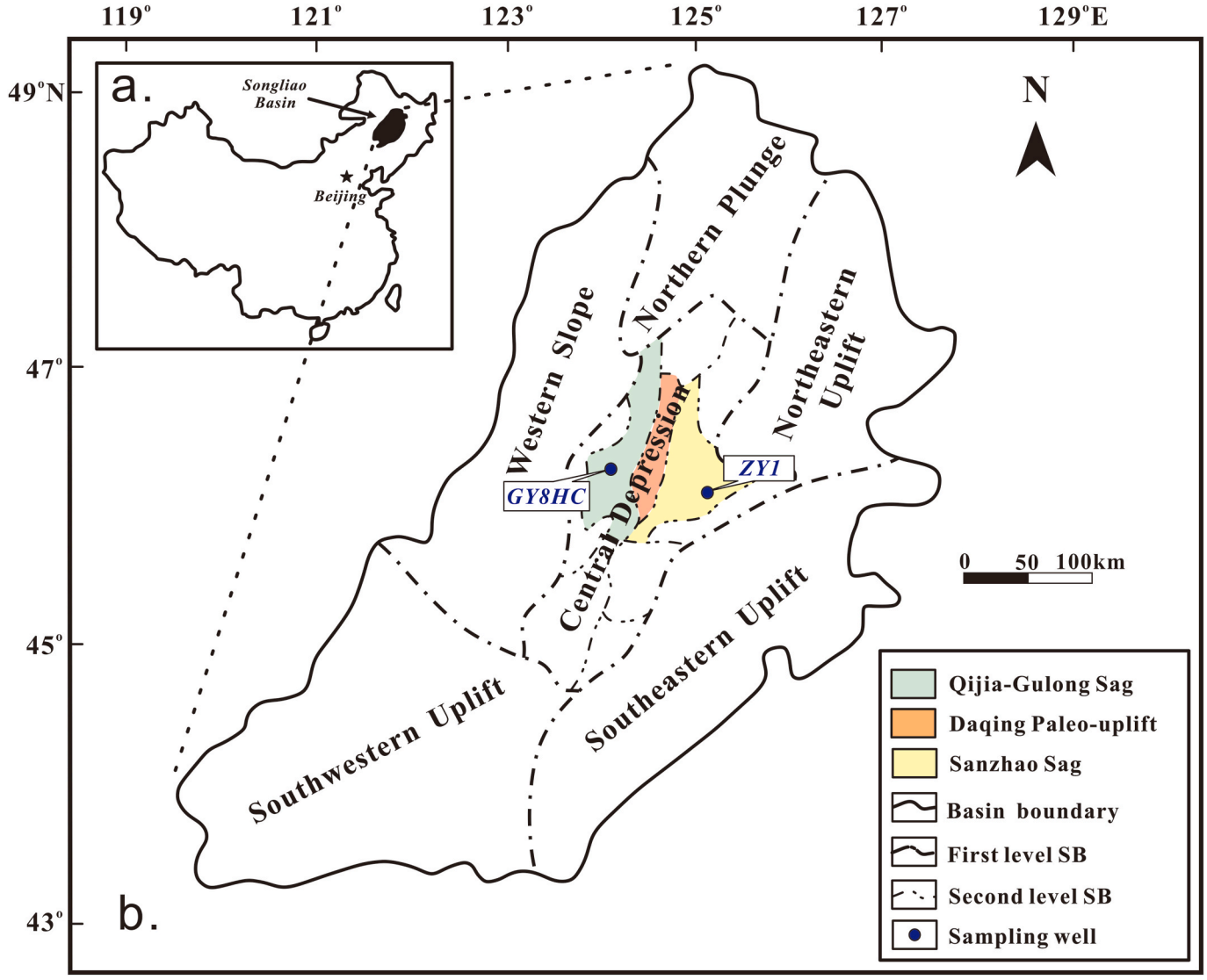

Fig. 1. (a) Location of the Songliao Basin in China. (b) Geological background of the Songliao Basin and the sampling well locations (modified after Chen et al., 2022). Note: SB represents structural unit boundary.

The result of this study provides a distinctive perspective through which to understand the climatic effects of marine incursions on mass accumulation of organic matter in continental basins. This study also provides key insights for predicting "sweet spots" for shale oil exploration in the Qingshankou Formation of the Songliao Basin.

2. Geological setting

The Songliao Basin in NE China developed an almost complete Cretaceous succession (Huang et al., 2013). The basin spans roughly 750 km in length and 350 km in width, with an area of approximately 260 000^2 km (Hou et al., 2000). The basin can be divided into six structural units (Fig. 1), the Northern Plunge zone, the Western Slope zone, the Central Depression zone, the Northeast Uplift zone, the Southeast Uplift zone, and the southwest uplift zone based on the tectonic evolution (Yang et al., 1985; Huang et al., 2013). Among them, the Central Depression zone stands out for hosting the most significant oil and gas-bearing tectonic units, such as the Gulong Sag, Daqing Uplift, Sanzhao Sag, Chaoyanggou Terrace, and Changling Sag (Feng et al., 2010). Particularly, the Gulong Sag and Sanzhao Sag are the main hydrocarbon-producing sags which are located in the west and the east of the Central Depression (Cao et al., 2020).

During the Cretaceous, the Songliao Basin was a large rift basin characterized by two episodes of extensive semi-deep to deep lake facies (the depth greater than 20 m) (Li et al., 2018), contributing to the deposition of the Qingshankou and Nenjiang formations (Gao and Cai, 1997). The Qingshankou Formation (K_2qn) was deposited in a semi-deep lake facies that was periodically affected by marine incursions, a phenomenon that occurred concomitant with global rise in sea levels (Feng et al., 2011; Huang et al., 2013). The Qingshankou Formation can be subdivided into three members (K_2qn^1, K_2qn^2, and K_2qn^3) based on lithologic characteristics. Among them, the K_2qn^1 is the major oil-bearing source rock. The paleolake reached its maximum area of nearly 7×10^4 km^2 during this time of period under the influence of marine incursions (Wang et al., 2016; Cao et al., 2021). Members 2 and 3 of the Qingshankou Formation (K_2qn^{2+3}) were deposited during a period of lake regression, which resulted in a reduced water body of the paleolake. The clastic input gradually increased and contributed to gray mudstones and interbedded siltstones during the deposition of K_2qn^{2+3}(Fig. 2). From the high precision biostratigraphic zonation and

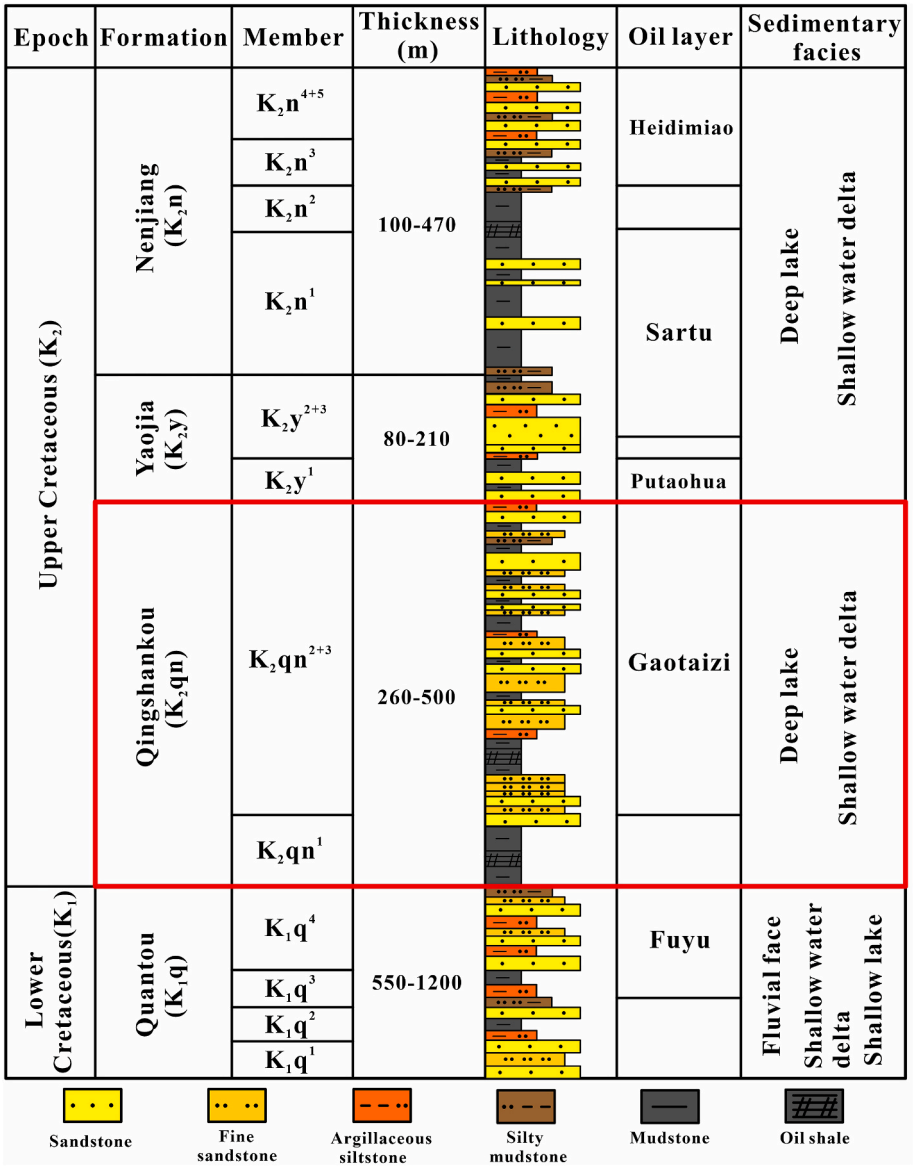

Fig. 2. Lithostratigraphic units, thickness and sedimentary facies of the Lower and Upper Cretaceous of the Songliao Basin (modified after Cao et al., 2021). Note: The red line highlights the Qingshankou Formation.

the chronostratigraphic framework via high quality U-Pb zircon radiometric ages, the duration of the K_2qn^1 is about 0.94 myr (from 91.37 to 90.44 Ma) (Wang et al., 2013b). In addition, the average sedimentation rate in K_2qn^1 in the Songliao Basin was 9.8 cm/kyr (Wang et al., 2013b).

3. Sampling and methods

Cores were sampled in this study from Well GY8HC (117 samples) located in the Gulong Sag and Well ZY1 (251 samples) located in the Sanzhao Sag, respectively (Fig. 1). Cores are continuous and span the entire K_2qn^1 and the lower part of the K_2qn^{2+3}. All samples within the cores were collected for total organic carbon (TOC), rock-eval pyrolysis, along with major and trace element analyses based on well log and lithological characteristics, including information on rock type variations, color, hardness, and mineral composition from published literature. More samples were collected from the carbonate-rich intervals in Well ZY1 to investigate the influence of marine incursions. Prior to conducting TOC and geochemical analyses, all samples were ground to a homogenous powder.

Thirty and forty samples were obtained from wells GY8HC and ZY1 for petrographic observations according to the variations in lithological characteristics. The thin sections were examined using a Nikon Optiphot petrographic microscope for the investigation of sedimentary structures. Organic matter characteristics were observed under fluorescence microscope (Leica DM4500P) at the State Key Laboratory of Petroleum Resource and Prospecting, China University of Petroleum-Beijing (CUPB).

The total organic carbon (TOC) content of all samples was quantified utilizing a Costech ECS 4010 combustion elemental analyzer, particularly after decarbonation, at the State Key Laboratory of Petroleum Resource and Prospecting, CUPB. Quality control protocols were applied to one out of every ten samples, which included duplicate samples, evaluation of certified standard materials (acetanilide), and assessment of blank samples. The analytical precision demonstrated an accuracy exceeding ±0.1 wt% for TOC measurements.

A total of 114 and 144 core samples were analyzed for rock-eval pyrolysis at the State Key Laboratory of Petroleum Resource and Prospecting, CUPB. In the analyzer, the samples underwent heating to a temperature of 300 °C and maintained for 3 min, then the temperature was increased at a rate of 25 °C per minute to reach 650 °C. After that, S1 (free hydrocarbon) and S2 (thermal cracked kerogen) are the output parameter peaks reported in mg HC/g. Hydrogen index (HI) is reported as S2/TOC × 100% of the sample (Lafargue et al., 1998).

The determination of major and trace elements was carried out using X-ray fluorescence spectroscopy (XRF) with a Thermo Scientific Niton XL3t GOLDD + Series Environmental Analyzer at Research Institute of Petroleum Exploration and Development, China National Petroleum Corporation. The unprocessed XRF data were subsequently standardized using ThermoNitonNDTr software. The analytical precision for all major elements exceeds 2%, and the precision and accuracy were estimated to be better than 5% for trace elements, respectively.

To determine the Sr isotopic ratios, 23 and 33 carbonate-rich samples were collected from wells GY8HC and ZY1, respectively, based on petrographic observations. Firstly, the separation of Sr was performed on a cation exchange column to minimize interference from isobaric impurities like Rb in mass spectrometry analysis. For details of separation procedure, refer to Sattouf et al. (2007). The Sr ratios were measured using Thermal Ionization Mass Spectrometry at the Institute of Geology and Geophysics, Chinese Academy of Science. The obtained ratios were normalized to a reference value of $^{86}Sr/^{86}Sr = 0.1194$. To assess the measurement accuracy, the NBS 987 standard was repeatedly measured, resulting in an average value of 0.710265 ± 0.000012 (n = 10), respectively.

4. Results

4.1. Core description

The core thickness of the GY8HC core and the ZY1 core are approximately 152 m and 125 m, respectively. The K_2qn^1 was primarily composed of dark gray to black clayey shale with abundant pyrite. Microfractures can be observed in this member (Fig. 3a), which are often filled with oil, resulting in frequent occurrences of oil streaks and patches and even visible oil exsolution in some samples (Fig. 3b).

Samples from the GY8HC core predominantly consist of thin shale layers interbedded with sandstone, silty shale, displaying stratification with features such as parallel, horizontal, and cross-bedding. In the K_2qn^{2+3}, sandstone interlayers are particularly well-developed, reaching up to 20 m in cumulative thickness, and include sedimentary structures such as convolute bedding (Fig. 3c), wavy lamination, and sandstone lenses. In contrast, the ZY1 samples are characterized by more extensive dolomitic and crystalline limestone interlayers (Fig. 3d), with a total thickness of 11 m. The samples of K_2qn^1 are mainly composed of dark and grayish-black shales, frequently interbedded with micritic limestone (Fig. 3e). Some samples exhibit sedimentary features like burrows and shelters that were produced by bottom-dwelling animals (Fig. 3f).

4.2. Petrographic observation

4.2.1. Sedimentary characteristics

Under microscopic observation, the Qingshankou Shale exhibits substantial heterogeneity in both texture and composition within the study area. The Qingshankou Shale in the GY8HC core consists of black shales interbedded with silty mudstones, while the ZY1 core contains gray-black shales interbedded with fossiliferous limestones. Based on laminae characteristics, the sedimentary structure and contact relationship with minerals, three types of laminar structures were identified as horizontal laminae, wavy laminae, and lenticular laminae.

Horizontal laminae can be divided into two types based on the mineral compositions. In general, felsic-clay horizontal laminae (Fig. 4a) are widely distributed in the GY8HC core site, while calcareous-clay horizontal laminae (Fig. 4b) are mainly developed in the ZY1 core site. The clay minerals are distributed as micritic, with calcite-filled in the microfractures.

Wavy laminae are mainly characterized by two types: felsic-clay wavy laminae (Fig. 4c) and calcareous (shell)-clay wavy laminae (Fig. 4d). These laminae exhibit a sinuous form, occasionally indicating hydrodynamic conditions, with significant thickness variations. They primarily consist of alternating sequences of clay bedding with fragmented feldspar or calcareous bedding. In the K_2qn^1, it is common to find shell fragments distributed layer-wise, with distinct, uniformly-sized particles typically appearing ellipsoidal.

Lenticular laminae can be classified into felsic-lenticular structures and calcareous-lenticular structures based on the mineral composition. Felsic lenses vary in size, ranging from 5 mm for larger ones down to 50 μm for smaller ones (Fig. 4e). Organic matter develops in the form of layers surrounding the feldspar lenses. Calcareous lenses in biological shells with the sizes typically between 200 μm and 500 μm, and tend to cluster, orientally arranged within organic bedding layers (Fig. 4f). Vertically, lenticular laminae are predominantly found in the K_2qn^{2+3}. Under the microscope, the ZY1 core samples show a higher abundance of intact shell fossils, whereas in the GY8HC core, many shells have been dissolved, with feldspar or calcium minerals filling their edges.

4.2.2. Organic matter characteristics

The organic matter of the Qingshankou shale, primarily originate from lacustrine algal and microsporinite (Fig. 5a and b), with content ranging significantly across different cores. These components exhibit diverse shapes, ranging from 10 to 50 μm, with an average size of around

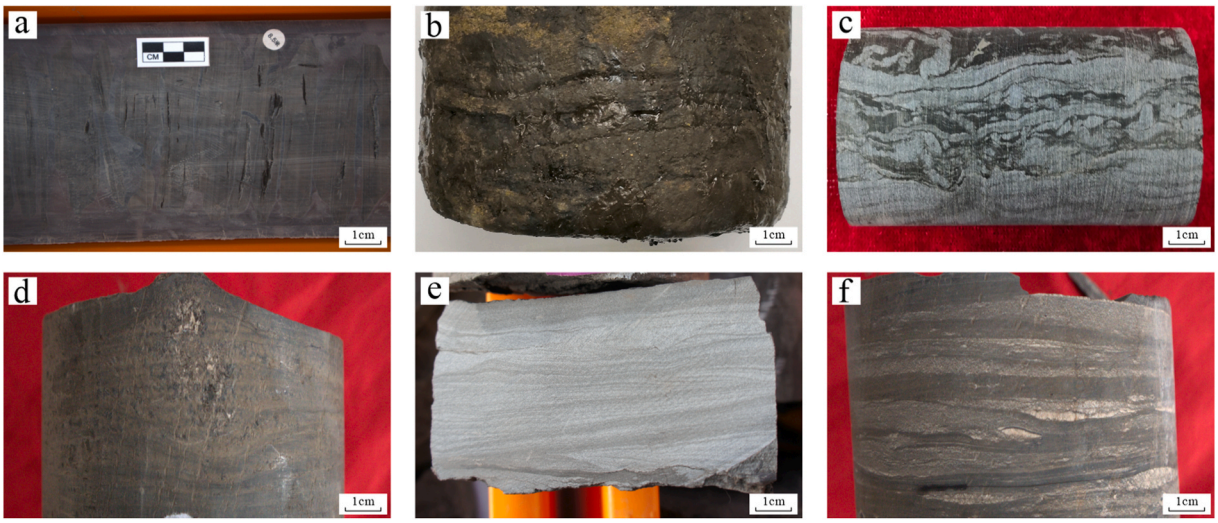

Fig. 3. Core characteristics of the Qingshankou Formation. (a) Dark gray to black clayey shale with microfractures, Well ZY1, 2039.6 m. (b) Oil streaks and patches in black clayey shale, Well GY8HC, 2515.9 m. (c) Observation of convolute bedding in gray shale, Well GY8HC, 2440.1 m. (d) Interbedded dolomitic and crystalline limestone layers, Well ZY1, 1980.1 m. (e) Micritic limestone interlayered with grayish-black shales, Well ZY1, 1954.1 m. (f) Burrow-fillings and shelters in Well ZY1, 1998.1 m.

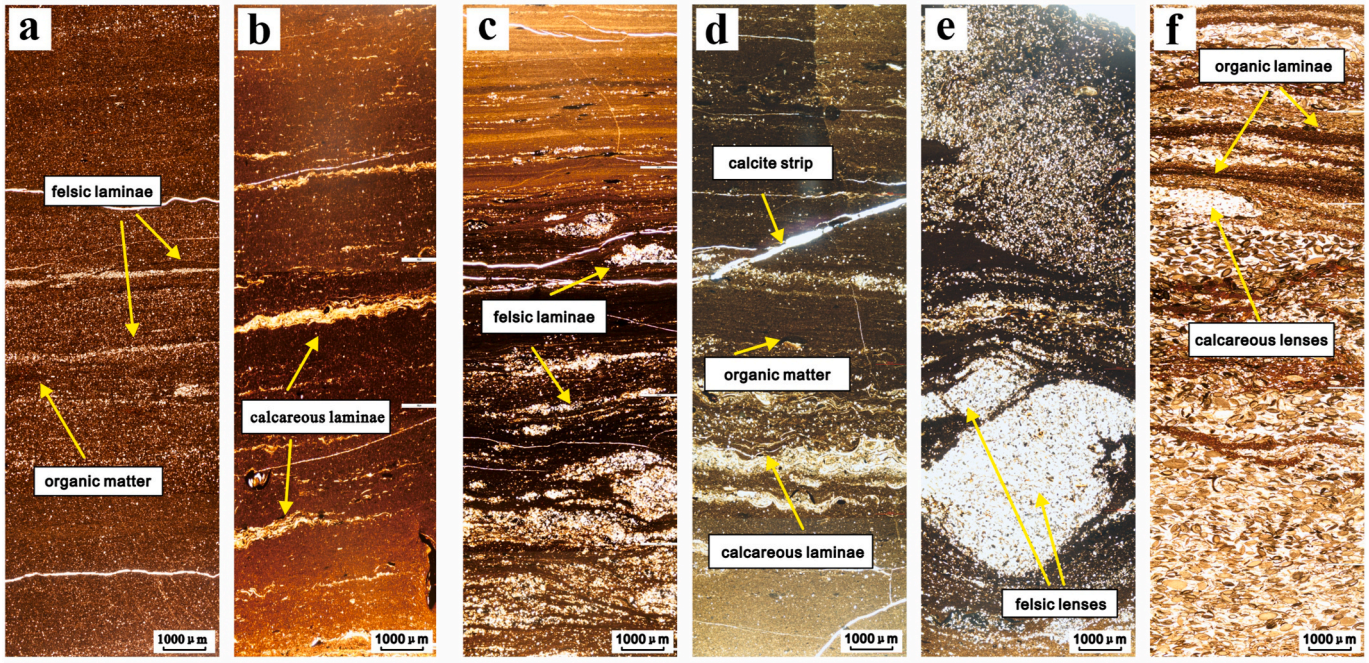

Fig. 4. Microscopic observation of laminar structures of the Qingshankou Formation. (a) Felsic-clay horizontal laminae in Well GY8HC, 2485.4 m. (b) Calcareous-clay horizontal laminae in Well ZY1, 1998.3 m. (c) Felsic-clay wavy laminae in Well GY8HC, 2410.3 m. (d) calcareous (shell)-clay wavy laminae in Well ZY1, 1973.2 m. (e) Felsic lenses in Well GY8HC, 2470.4 m. (f) Calcareous lenses are interbedded within organic bedding layers, Well ZY1, 1961.2 m.

20 μm. Microsporinite, derived mainly from plant spores, are commonly seen as round, oval, flat-lamellar, or worm-like morphologies (Fig. 5c), occasionally forming small clusters of spores. In addition, bituminites can be identified under transmitted light, which is a dominant organic component in marine shales, possesses significant hydrocarbon generation potential. The organic matter in GY8HC samples is mainly sapropel, predominantly composed of alginite with total amount over 50%. These are observed as algal-rich laminae within black shales and dark mudstones. In contrast, the ZY1 samples contain a certain quantity of the exinite (20%–40%) (Fig. 5d, e, f). In summary, organic matter type I and II are dominant in both wells, while ZY1 well has higher Type II_1 kerogen with a lesser amount of Type I.

4.3. Source rock characteristics

4.3.1. Total organic carbon content (TOC)

The TOC values show different patterns in both wells (Figs. 6 and 7). The overall TOC values are higher in the ZY1 core samples than those from GY8HC. In the K_2qn^1, the TOC values range between 0.39% and 8.23%, with an average of 2.64% in the ZY1, while the TOC basically fluctuate between 0.61% and 3.74%, with an average of 1.73% in the GY8HC. The average TOC values of K_2qn^{2+3} are 1.21% and 2.29% in the GY8HC and the ZY1 core samples, respectively. In addition, the TOC values display stratigraphic change in the ZY1 core, with low values at the base and reach to as high as 8.3% in the middle of K_2qn^1.

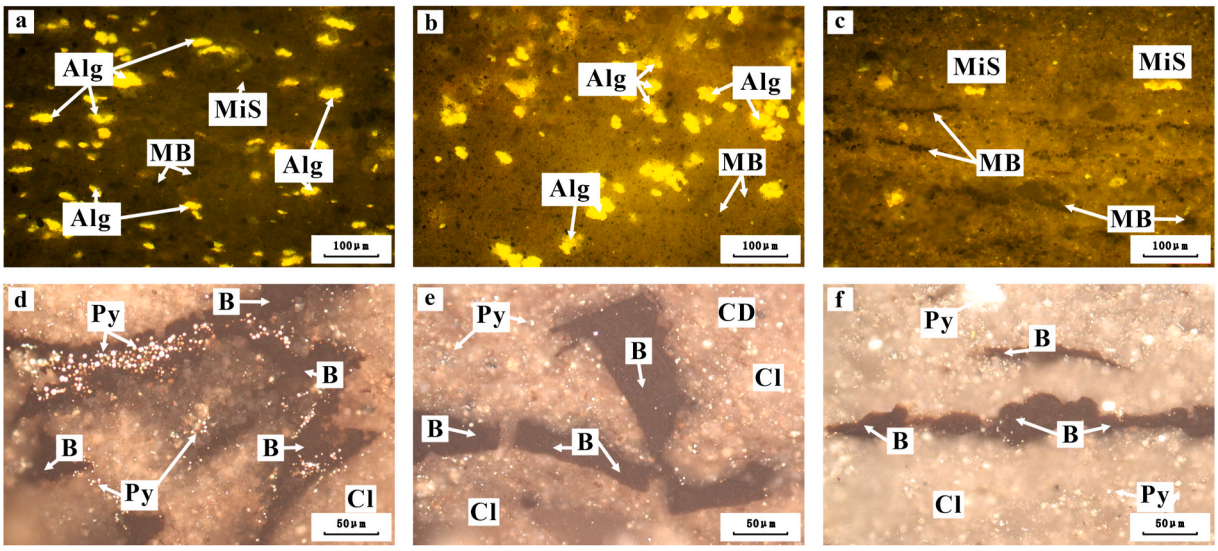

Fig. 5. Maceral identification of the Qingshankou Formation. (a) and (b) Alginite and microsporinite are concentrated in laminated mineral bituminite, exhibits bright yellow fluorescence, Well ZY1, 1982.5 m, 2014.3 m. (c) Microsporinite within mineral bituminous under fluorescent light, Well GY8HC, 2458 m. (d), (e) and (f) Abundant bituminites occur within black shales and dark mudstones, pyrite framboids are observed under polarized light, Well ZY1, 2026.1 m, 2012.5 m, and 2034.2 m. Note: Alg: alginate; MiS: microsporinite; MB: mineral bituminite; Py: pyrite; B: bituminite; Cl: clay; CD: vitrodetrinite.

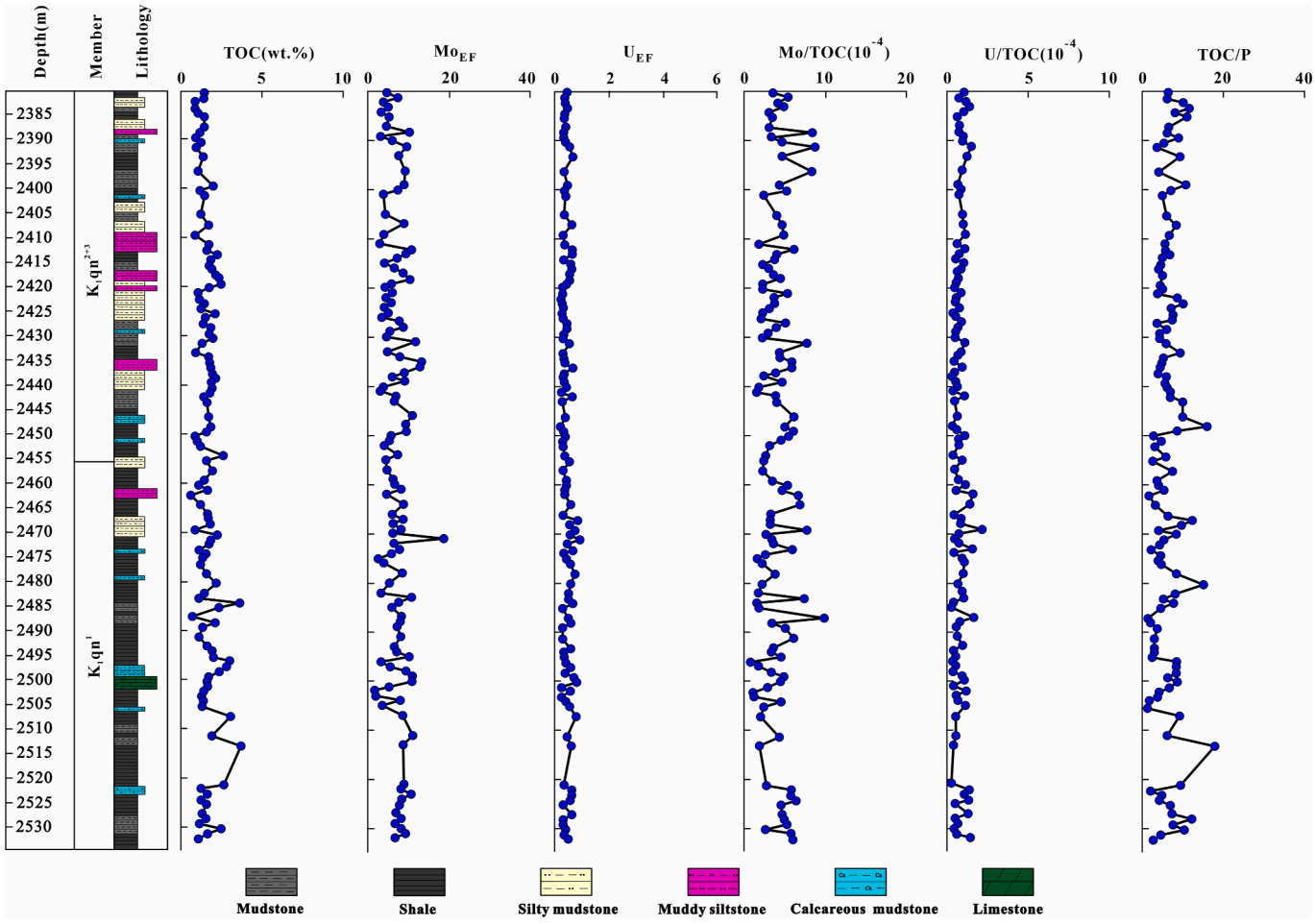

Fig. 6. Profiles of total organic carbon (TOC), enrichment factors of Mo and U (Mo_{EF}, U_{EF}), Mo/TOC, U/TOC, and TOC/P of the Qingshankou samples, the GY8HC core.

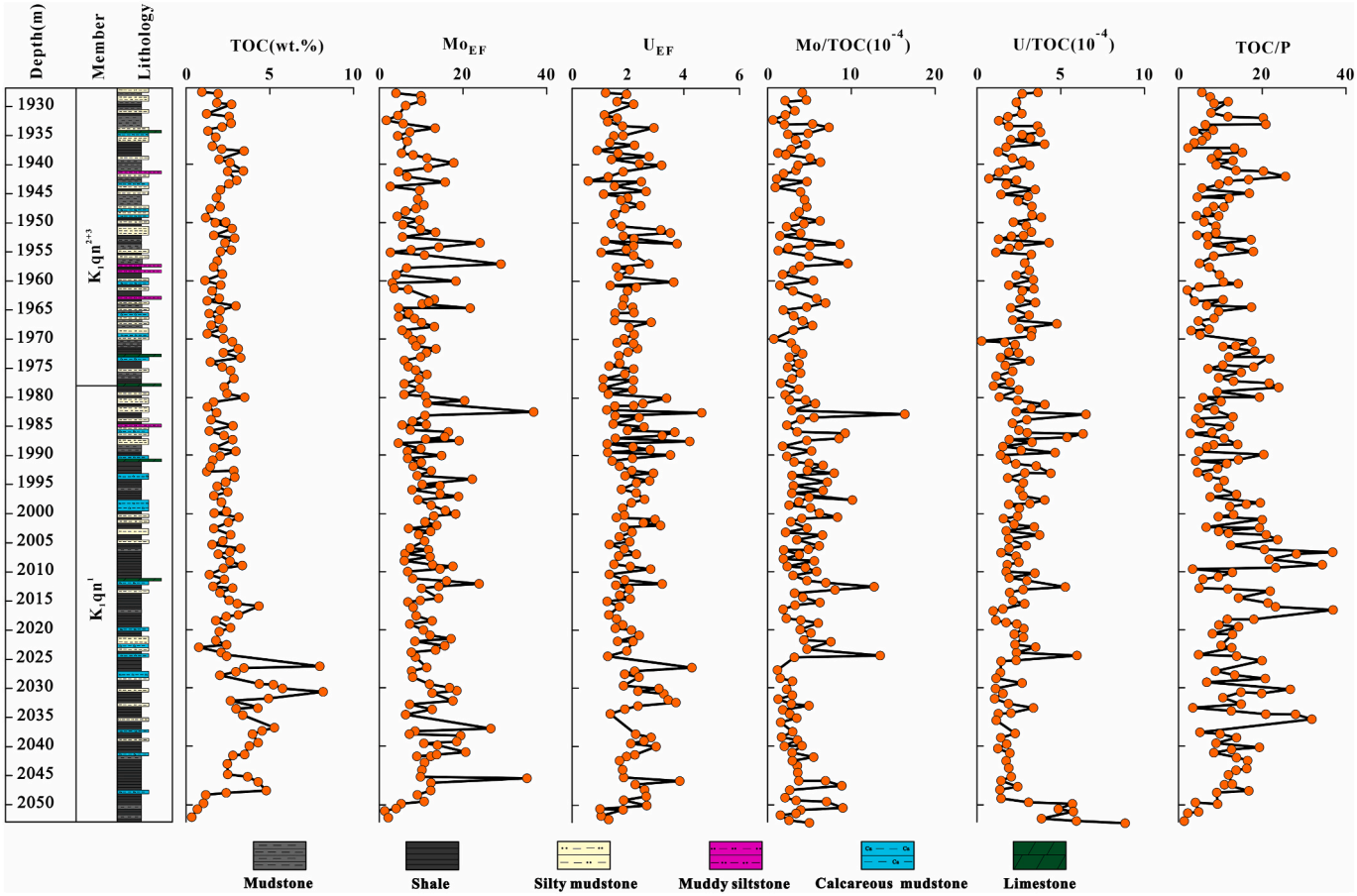

Fig. 7. Profiles of total organic carbon (TOC), enrichment factors of Mo and U (Mo_{EF}, U_{EF}), Mo/TOC, U/TOC, and TOC/P of the Qingshankou samples, the ZY1 core.

Subsequently, a gradual upsection decrease in TOC is found throughout the upper part of K_2qn^1 and remain consistently low values in K_2qn^{2+3}.

4.3.2. Hydrogen index (HI)

The HI values is another critical parameter for assessing the hydrocarbon potential of source rocks. The overall HI values are higher in the ZY1 core samples than those from the GY8HC (Figs. 8 and 9). In the ZY1, the HI values range between 255 and 979 (mg HC/g TOC), with an average of 505 (mg HC/g TOC) in the K_2qn^1, while the HI values fluctuate between 102 and 971 (mg HC/g TOC), with an average of 574 (mg HC/g TOC) in the K_2qn^{2+3}, respectively. However, the average HI values of the GY8HC Well are 196 (mg HC/g TOC) in the K_2qn^1 and 289 (mg HC/g TOC) in the K_2qn^{2+3}.

4.4. Major and trace element data

The major and trace elements of GY8HC and ZY1 core samples are presented in Supplementary Tables S1 and S2. For redox sensitive elements, molybdenum (Mo) and uranium (U) concentrations and enrichment factors (Mo_{EF} and U_{EF}) of all samples were calculated to exclude the influence of detrital influx (PAAS-normalized EF following Wedepohl, 1991). Specifically, U_{EF} is expressed as $(U/Al)_{sample}/(U/Al)_{PAAS}$, whereas Mo_{EF} is expressed as $(Mo/Al)_{sample}/(Mo/Al)_{PAAS}$. In this study, Mo_{EF} and U_{EF} show subtle variations in the well GY8HC (Fig. 6). These elements are highly concentrated at the base of ZY1 (Fig. 7). In addition, the average value of Mo_{EF} (6.17) and U_{EF} (0.41) from the GY8HC core samples is much lower than that of the ZY1 (Mo_{EF}: 9.18; U_{EF}: 1.8). In the ZY1 core, the trace elements such as boron (B), barium (Ba), strontium (Sr) and copper (Cu) display clear changes from the K_2qn^1 to the K_2qn^{2+3}. The K_2qn^1 is characterized by relatively high concentrations of B and Cu, with averages of 101.4 ppm and 36.9 ppm, respectively, and low concentrations of Ba and Sr with averages of 28.3 and 356.9 ppm, respectively. In contrast, the K_2qn^{2+3} is characterized by significantly low concentrations of B (averaging = 77.8 ppm) and Cu (averaging = 28.3 ppm), high concentrations of Ba (averaging = 524.4 ppm) and Sr (averaging = 332.9 ppm). However, B, Ba, Sr and Cu contents in the GY8HC core show no obvious patterns throughout most of the Qingshankou Formation.

4.5. Sr isotopic compositions

The $\delta^{87}Sr$ values in GY8HC core samples are relatively stable throughout the Qingshankou Formation (Fig. 8), ranging between 0.71124‰ and 0.71298‰ (averaging = 0.71194 ± 0.00049‰). However, in the ZY1 core, the $\delta^{87}Sr$ values of the K_2qn^1 are generally lower (averaging = 0.71002 ± 0.00057‰) than those in the K_2qn^{2+3} (averaging = 0.71220 ± 0.00092‰) (Fig. 9). In particular, the $\delta^{87}Sr$ values present a decreasing upward trend in the K_2qn^1 and reach to the minimum value in the middle of this member.

5. Discussion

5.1. Variations in sedimentary environment between two sags

The development of laminar structures is closely related to sedimentary environment. Abundant calcareous minerals, shell fragments and the alternating layers of calcareous material and organic matter in the ZY1 core site (i.e., the Sanzhao Sag) might suggest the occurrence of marine incursions (Huang and Huang, 1998; Xi et al., 2011). Under this circumstance, the seawater influx facilitated the development of

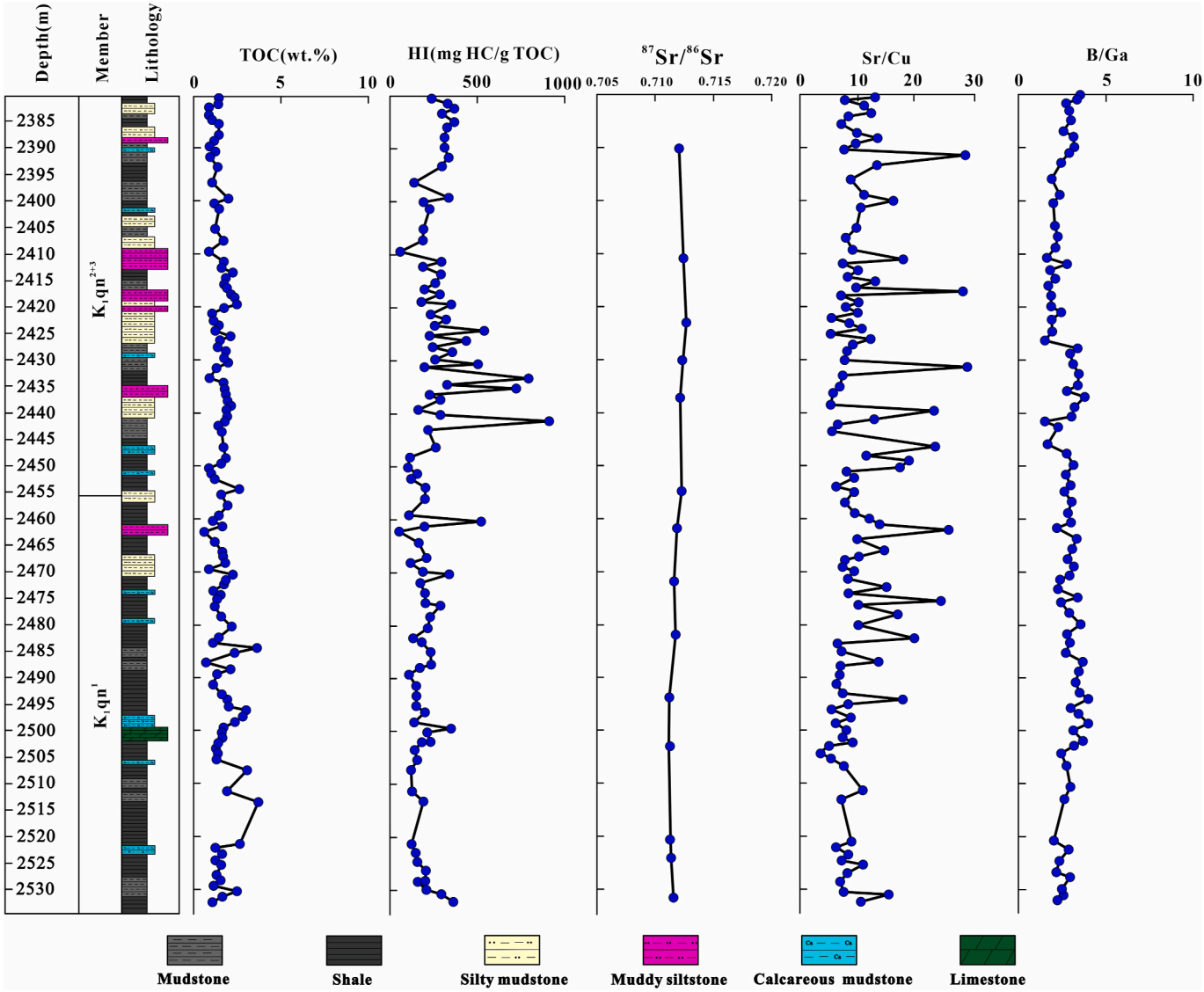

Fig. 8. Profiles of total organic carbon (TOC), hydrogen index (HI), $\delta^{87}Sr$, ratios of Sr/Cu, and B/Ga of the Qingshankou samples, the GY8HC core.

carbonates. In contrast, the GY8HC core site (Gulong Sag) is closer to the sediment source, which is evidenced by the development of abundant felsic laminae, with small-scale ripple structures and mineral grain alignment (Lan et al., 2013). Such sedimentary characteristics reflects increased terrestrial input and stronger water dynamic strength during the deposition. This conclusion is also supported by the varied organic matter types across the different cores. The organic matter of the GY8HC core is mainly Type I, primarily originated from lacustrine algae with a small amount of microsporinite. The organic matter of the ZY1 core, however, composed a higher percentage of Type II_1, which is characterized by a certain quantity of exinite. The development of calcareous mudstones, shell fragments, and Type II_1 organic matter, consistently indicate episodic marine incursions during the deposition of the Qingshankou Formation in the Sanzhao Sag. Compared to the Sanzhao Sag, the K_2qn^1 of the Gulong Sag was deposited in semi-deep to deep lacustrine environment. The layers of silty mudstone and muddy siltstones in the K_2qn^{2+3} reflects increased terrestrial influx during this period.

5.2. Variations in redox conditions between two sags

5.2.1. Evidence from TOC/P ratios

The phosphorus (P) cycle is governed by benthic redox conditions, particularly under anoxic bottom water conditions. In such settings, a considerable amount of P is released into the overlying water column through the reductive dissolution of iron oxyhydroxides within sediments (Algeo and Ingall, 2007; Algeo and Li, 2020; Algeo and Liu, 2020). Abundant P can also be released as a result of organic matter degradation under oxic-suboxic conditions, and is effectively preserved in sediments (Sageman et al., 2003; Algeo and Ingall, 2007). Consequently, sediments deposited under anoxic conditions typically exhibit higher TOC/P ratios compared to those formed under oxic-suboxic environmental conditions (Algeo and Ingall, 2007).

The TOC/P ratios through the ZY1 and GY8HC cores are mostly characterized by low TOC/P ratios (GY8HC: 6.43; ZY1:12.19, in average). According to the redox threshold established by Algeo and Ingall (2007), which distinguishes between oxic, suboxic, and anoxic conditions based on TOC/P ratios exceeding 50 and 100 respectively. Therefore, the Qingshankou Formation were deposited under oxic bottom waters and suboxic porewaters just below the sea water interface (SWI). It is worth noting that, the TOC/P ratios increase up to 37.37 in the middle of K_2qn^1 the in ZY1 core (~2005 m–2020 m), indicating a decreasing oxygen level during the depositional history of these intervals.

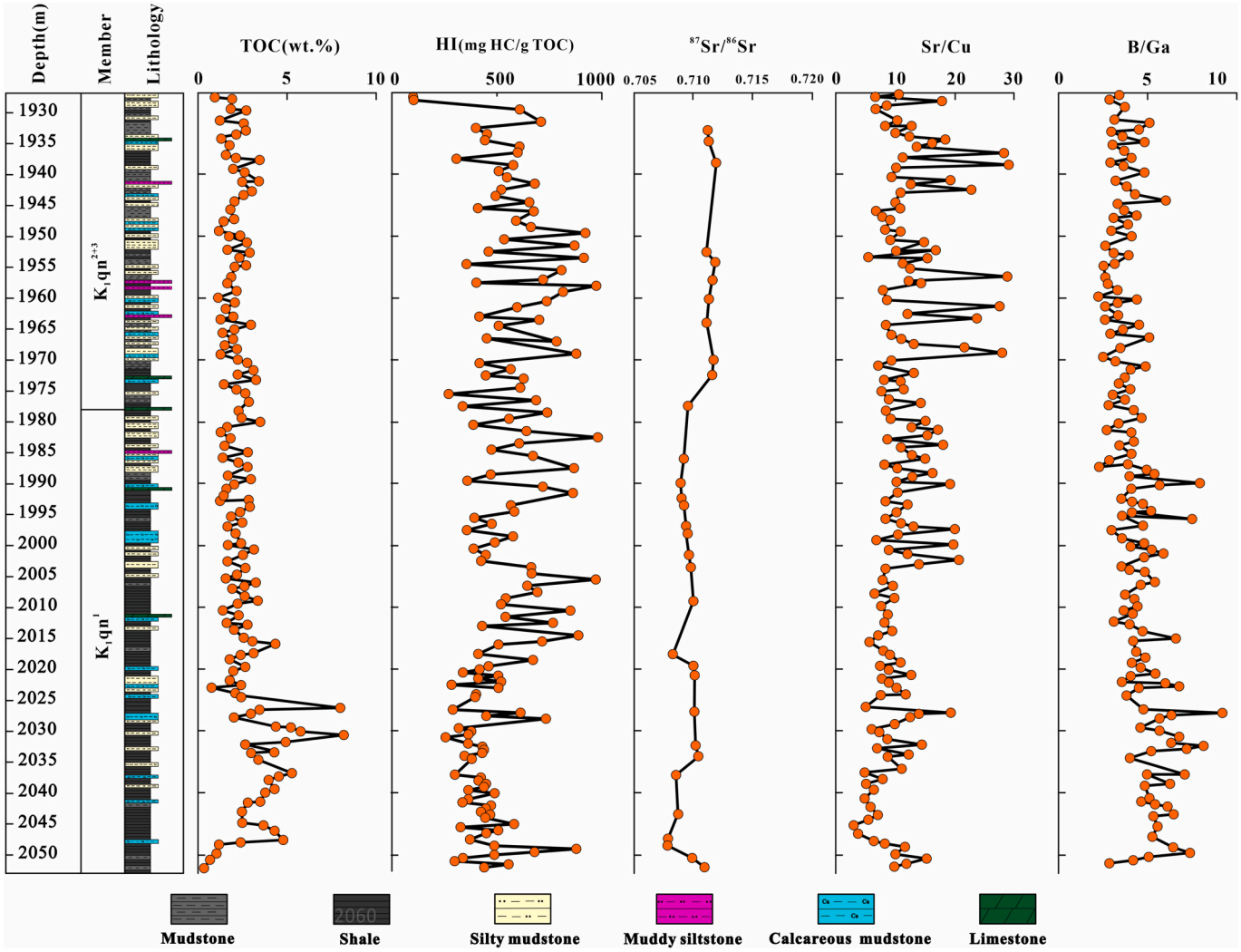

Fig. 9. Profiles of total organic carbon (TOC), hydrogen index (HI), $\delta^{87}Sr$, ratios of Sr/Cu, and B/Ga of the Qingshankou samples, the ZY1 core.

5.2.2. Evidence from Mo_{EF} and U_{EF}

The enrichment of redox-sensitive trace elements in sediments are effective proxies in reconstructing the redox conditions of bottom water during deposition (e.g., Tribovillard et al., 2006, 2012; Chen and Sharma, 2016; Algeo and Li, 2020; Algeo and Liu, 2020). Among these elements, Mo and U exhibit exceptional importance and efficacy due to their markedly low concentrations in the upper continental crust (McLennan, 2001), but long residence times in seawater, reflecting their unique geochemical properties and geological behavior (Tribovillard et al., 2012). Furthermore, Mo and U are aqueous soluble in oxic conditions, however, in anoxic or euxinic environment, they are significantly concentrated through sedimentary uptake (Tribovillard et al., 2006). Consequently, the enhancements of Mo and U in sedimentary deposits are interpreted as authigenic accumulation of these elements from seawater, highlighting the differential biogeochemical behaviors of these elements under varying redox conditions.

In this study, the authigenic enrichments of Mo and U are quantified using Al-normalized enrichment factors (EFs) to mitigate the impact of detrital influx. For instance, U_{EF} is determined by contrasting the concentration of U in the sample, normalized to Al, against the U concentration in the Post-Archean Australian Shale (PAAS) standard (McLennan, 1989). $U_{EF}>3$ represents an enriched concentration relative to PAAS, whereas $U_{EF}>1$ represents a depleted concentration (Tribovillard et al., 2012). In the both cores, the U_{EF} exhibit relatively low values (average = 0.46 ± 0.15 in GY8HC; average = 2 ± 0.73 in ZY1) (Figs. 6 and 7), even in the organic-rich shale intervals, indicating oxic conditions throughout the deposition of the Qingshankou Formation. This supplies further validation for the redox state assessment reliant upon the TOC/P ratio analysis. In summary, the low values of Mo_{EF} and U_{EF} indicate that the depositional system was oxic-suboxic at the core sites of GY8HC and ZY1. Furthermore, the Mo_{EF} and U_{EF} values exhibit abrupt increases (Mo_{EF}: 43.60; U_{EF}: 3.87) at the base of the K_2qn^1 in ZY1 core (Fig. 7). After that, these two values show several positive excursions throughout the Qingshankou Formation. It is worth noting that the higher Mo_{EF} and U_{EF} were observed in some intervals, such as Mo_{EF} is 23.76 at depth of 2012 m, U_{EF} is 4.30 at the depth of 2026 m. The elevated Mo_{EF} and U_{EF} values might reflect weakly oxic bottom waters and suboxic to mildly euxinic porewaters below the SWI. As a result, a bit of Mo and U enrichments in the ZY1 core samples suggests that the depositional condition was more reducing at the core site of ZY1 than those of GY8HC. Another possible explanation for the relatively low Mo_{EF} and U_{EF} values in the GY8HC core site might be attributed to the restricted circulation and the consequent depletion of Mo and U in the Gulong Sag. The watermass was too well-oxygenated to permit much trace metal uptake, the TOC/P data further support this interpretation.

5.2.3. Evidence from Mo/TOC and U/TOC

The Mo/TOC and U/TOC ratios in sediments serve as indicators for reconstructing the redox conditions at the time of sedimentation. In the scope of this research, Mo and U have been normalized to TOC to

exclude the influence of organic matter (Figs. 6 and 7). Previous research indicated a strong correlation between Mo and U concentrations and organic matter within sediments, functioning as a carrier for their transport from the aqueous phase to sediments under anoxic/euxinic conditions (Tribovillard et al., 2006; Peng, 2022). As a result, the ratio of two authigenic components (i.e., Mo/TOC, U/TOC) act as more reliable proxies for interpreting changes in paleoenvironmental conditions (Algeo and Lyons, 2006; Abshire et al., 2020; Cao et al., 2021; Peng, 2022). The generally higher Mo/TOC and U/TOC ratios observed in Well ZY1 (Figs. 6 and 7) provide further evidence that the Sanzhao Sag exhibited slightly more reducing conditions just below the SWI, allowing slightly higher trace metals uptake by the sediment. In particular, the average Mo/TOC and U/TOC values in mudstone and shale layers are ~1.1 × and ~2.5 × higher in the ZY1 well than those in the GY8HC well, respectively. This coherence has served to reinforce our hypothesis that the changes in redox conditions was the principal influence on the accumulation of authigenic Mo and U in the organic-rich shales between two wells, which is also supported by Mo_{EF} and U_{EF} values.

5.3. Variations in paleoclimate and paleosalinity between two sags

Paleoclimate not only influenced precipitation, chemical weathering, and water column stratification in paleolakes, but also controlled variations in salinity of the water column, which in turn governed the accumulation and preservation of organic matter in sediments (Martinez-Ruiz et al., 2015). The concentrations of strontium (Sr) and copper (Cu) are sensitive to paleoclimate, in which Sr tends to be enriched under arid and hot conditions. Thus, the ratio of Sr/Cu is a reliable proxy for reconstructing paleoclimates (Wang et al., 2022).

5.3.1. Evidence from Sr/Cu ratio

Sr concentrations ranged from 176 to 822 ppm, with Sr/Cu ratios of 4.14–37.78 in well GY8HC (Fig. 10a). In well ZY1, the Sr concentrations range between 142 and 954 ppm, with a Sr/Cu ratio varying from 3.17 to 34.98 (Fig. 10b). The crossplots from both wells suggest a semi-humid to semi-arid climate during the deposition of the Qingshankou Formation in both sags. Both sags present a slightly warm and humid, semi-humid to semi-arid climate during the deposition of the K_2qn^1. However, in the K_2qn^{2+3} more samples from the ZY1 Well are plotted in the semi-arid and arid climate than those from the GY8HC well. Thus, the paleoclimate in the Gulong Sag was relatively constant throughout the deposition of the Qingshankou Formation while in the Sanzhao Sag, the paleoclimate became dryer during the deposition of K_2qn^{2+3}.

5.3.2. Evidence from B/Ga ratio

Paleosalinity was also determined using B/Ga ratios in this study. In modern freshwater sediments, the median concentrations of B and Ga are 4.8 ppm and 3.8 ppm, respectively, leading to a B/Ga ratio of 1.29. In contrast, sediments from marine environments exhibit median concentrations of 300 ppm for B and 19 ppm for Ga, which consequently yield a B/Ga ratio of 15.3 (Wei and Algeo, 2020). The increased uptake of B in marine environments compared to freshwater settings is attributed to the high alkaline in saline waters (Spivack et al., 1987). Therefore, the B/Ga ratio of less than 3 indicates freshwater, 3–6 represents brackish water, and values greater than 6 in marine environments (Wei and Algeo, 2020). In the GY8HC Well, the median B/Ga ratio is 2.58 (0.78–4.00) with little variation throughout the Qingshankou Formation (Fig. 10c), whereas the median B/Ga ratio is 4.06 (2.09–10.04) in the ZY1 Well (Fig. 10d), suggesting higher salinity watermasses during the deposition at the ZY1 core site (i.e., Sanzhao Sag) relative to than those at the GY8HC core site (i.e., Gulong Sag). Particularly, elevated B/Ga

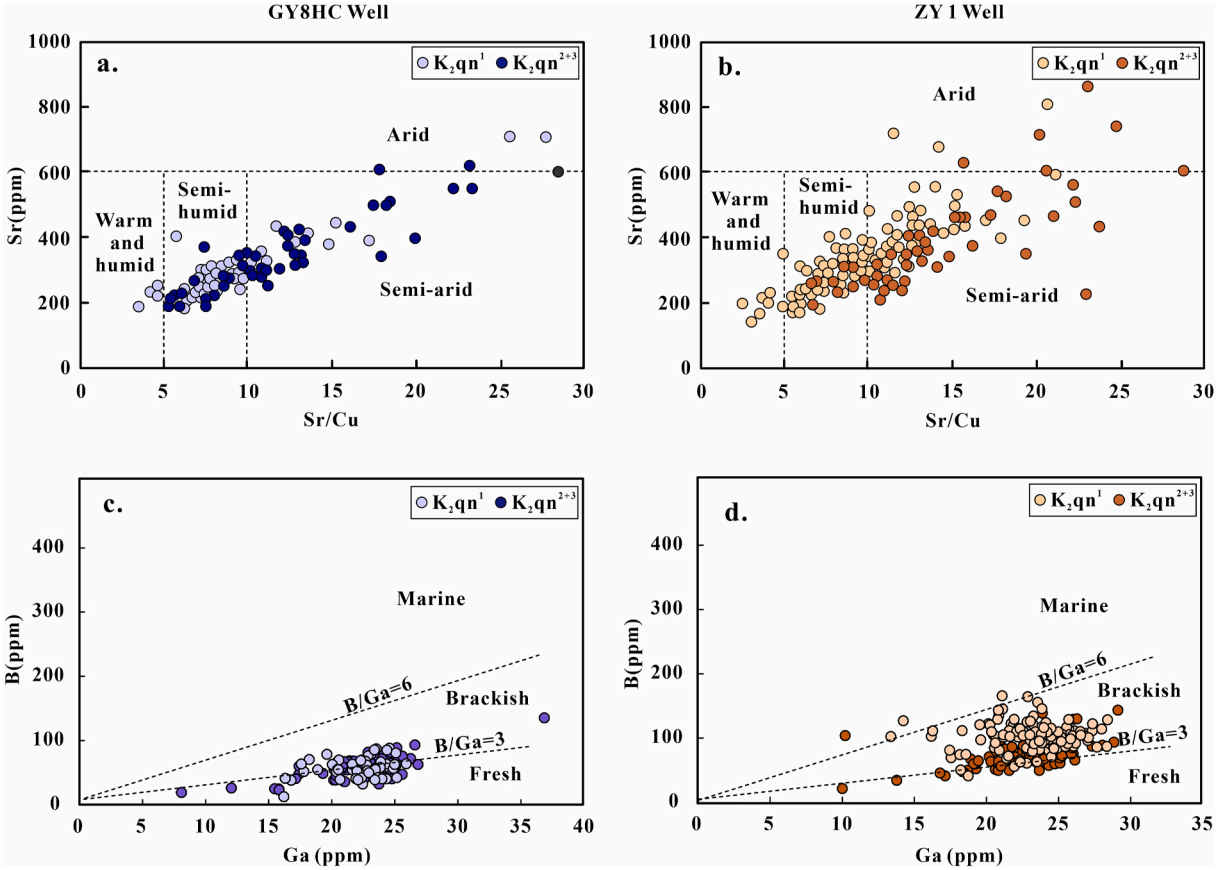

Fig. 10. The relationships between Sr and Sr/Cu, B and Ga in the GY8HC Well (a and c) and ZY1 Well (b and d) (according to Li et al., 2020; Wei and Algeo, 2020).

ratios can be observed in the K_2qn^1 of the ZY1 Well, with the changes in B/Ga ratios being coupled with the variations of Sr/Ba ratios. These two proxies both indicate the paleosalinity was brackish-to marine during the deposition of the K_2qn^1 in the Sanzhao Sag.

5.3.3. Evidence from Sr isotope

The isotope ratio of $^{87}Sr/^{86}Sr$ is recognized as one of the most stable isotopes on Earth, and it has been extensively employed as a reliable indicator for constraining the age of sedimentary rocks (Palmer and Elderfield, 1985). The rationale behind this application lies in the fact that the residence time of Sr in seawater is significantly longer by several orders of magnitude compared to the mixing time of seawater. Consequently, it is suggested that seawater maintains a uniform distribution of Sr isotopic composition throughout geological history (Peros et al., 2007; Bosio et al., 2020; Liu et al., 2023). The impact of terrestrial Sr input during the formation of lacustrine carbonates can markedly elevate the Sr isotopic compositions from the initial lake water value (Jacobsen and Kaufman, 1991). Thus, the Sr isotopes of carbonate precipitates can be used as proxy for the reconstruction of paleosalinity throughout the time of deposition (Ingram and DePaolo, 1993; Reinhardt et al., 1998; Peros et al., 2007).

The $^{87}Sr/^{86}Sr$ values of the calcareous mudstone samples in GY8HC Well range between 0.71124 and 0.71262, being close to the lacustrine carbonates. Specifically, these values are comparable to those found in the Late Triassic Yanchang Formation within the Ordos Basin, which exhibit $^{87}Sr/^{86}Sr$ values between 0.71122 and 0.71159 (Zhu et al., 2020), and the Lower Cretaceous Xiagou Formation in the Jiuquan Basin, is characterized by isotopic ratios from 0.71225 to 0.71781 (Wen et al., 2007). However, the $^{87}Sr/^{86}Sr$ values of the calcareous mudstone samples in ZY1 Well remain at 0.70774–0.71183 (Figs. 8 and 9), which are much lower than those of the GY8HC samples. Moreover, the $^{87}Sr/^{86}Sr$ values exhibit a descending trend in the K_2qn^1 of ZY1, culminating in a minimum value of 0.70774, which is closely comparable to the contemporaneous seawater isotopic ratio of 0.7074 (Bwire Ojiambo et al., 2003). As a result, the relatively low $^{87}Sr/^{86}Sr$ values might suggest a significant contribution from seawater. Previous studies suggested the concentration of Sr in seawater is significantly higher, about three orders of magnitude greater than in freshwater, and a minor mixture, constituting less than 10% of seawater, would lead to a large isotopic fractionation and thus contributing to a significant decrease in the Sr isotopic compositions of lake water (Liu et al., 2023). This conclusion is consistent with the evidence of B/Ga ratios as discussed above.

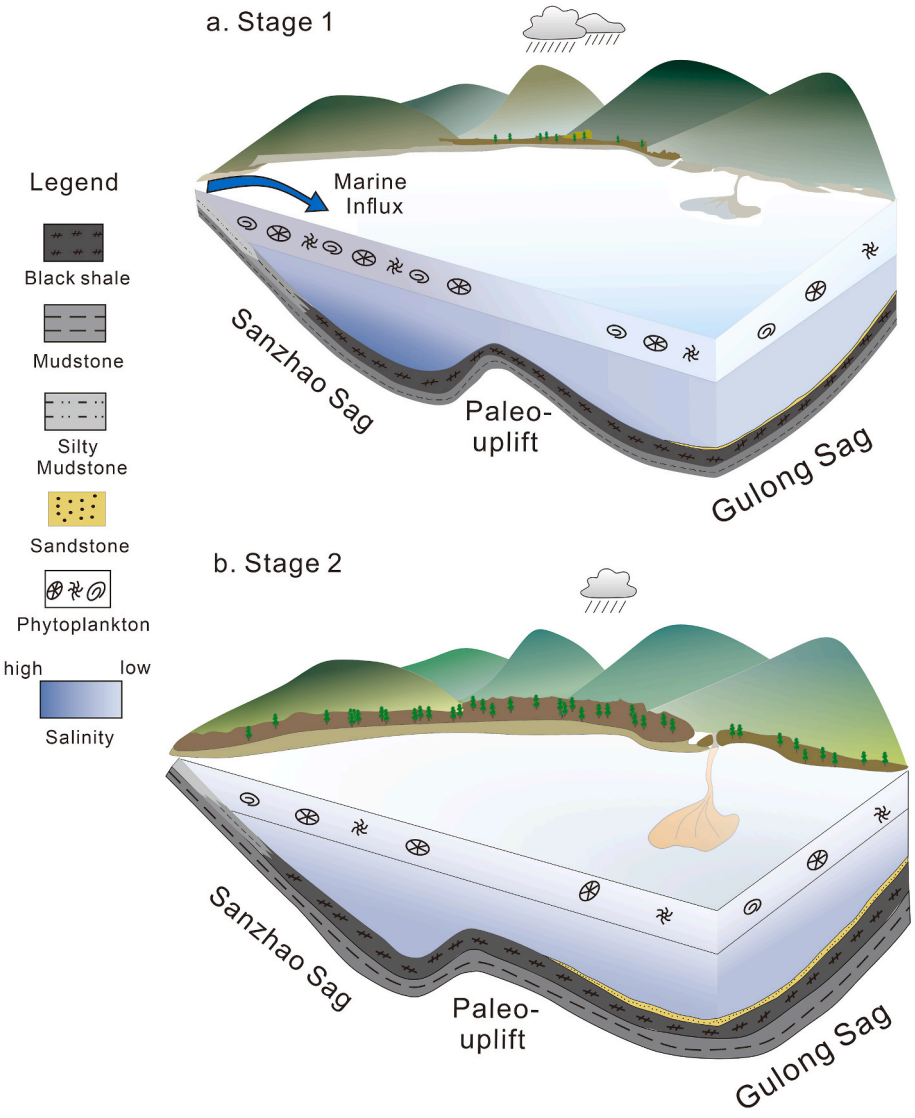

Fig. 11. Conceptual depositional model of the Qingshankou Formation in the Gulong and Sanzhao sags during (a) and after (b) the seawater incursion in the Central Depression in the Songliao Basin.

5.4. Depositional model of the Qingshankou Formation in two sags

The teleconnections between the global marine events to the continental margin basins is essential to influence the regional depositional conditions of the basins, and therefore promoted organic productivity and contributed to source rock formation in the basin (Barrera and Johnson, 1999; Wei et al., 2018; Xia et al., 2019; Xu et al., 2022). The evidence of sedimentary characteristics, geochemical elements and Sr isotopic compositions prove that the marine incursion episodes might have influenced the dynamics of Songliao paleolake water chemistry and led to variations in stratification, thereby impacting the burial of organic carbon across distinct sags within the Central Depression (i.e., Gulong and Sanzhao sags).

In this view, it was proposed that the depositional model of the Gulong and Sanzhao sags during the deposition of Qingshankou Formation exhibits two stages (Fig. 11). During the deposition of the K_2qn^1 (Stage 1), the stagnant watermasses of the Songliao paleolake were periodically disrupted by episodic intrusions of seawater, particularly in the Sanzhao Sag. The seawater flow overrode the land which blocked the paleolake and Paleo-Pacific Ocean, and concurrently introduced high salinity water and chemical elements (e.g., Ca, Mg, U and Mo) into the Sanzhao Sag. In this case, the calcareous limestones precipitated in thin layers within the Qingshankou Formation account for approximately 8% of the total thickness. This contrasts with the massive, hundreds of meters thick, and hundreds of kilometers laterally extensive carbonates that are originated through evaporation processes (Liu et al., 2023). In addition, the rising lake level and increasing salinity of the watermasses could have contributed to the stratification of water column. Such conditions probably created a natural barrier for the circulation of water (Werne et al., 2002), which was favorable for organic matter preservation. Meanwhile, the warm and humid climatic conditions facilitated the reproduction rates of the phytoplankton populations. The subsequent microbial decomposition of organic matter could have caused a consumption of oxygen in water column, leading to dyoxic conditions during the deposition of upper K_2qn^1. Consequently, the episodic seawater intrusions facilitated the deposition of thick sequences of black shale in the K_2qn^1 at the ZY1 core site. However, in the Gulong Sag, the seawater incursion was block by the paleo-uplift, a large anticlinal structural belt between the Gulong and Sanzhao sags. Under this circumstance, the Qingshankou Formation in the Gulong Sag was less affected by the episodic marine incursion events. This is supported by sedimentary features, organic matter characteristics and paleosalinity proxies (e.g., relatively high Sr isotopes, low B/Ga ratios). Furthermore, the Gulong Sag is proximate to the sediment source, leading to a greater receipt of terrestrial input. This condition is deemed unfavorable for the preservation of organic matter (Fig. 11a).

After the seawater incursion (Stage 2), the paleoenvironmental conditions became similar between the Gulong and Sanzhao sags. During the deposition of K_2qn^{2+3}, the paleoclimatic conditions exhibited recurrent transitions between semi-arid and semi-humid, which were generally drier than those prevailing during Stage 1. The lake level decreased after the seawater incursion and the redox condition was oxic, preventing organic matter preservation in the bottom waters of the Gulong Sag. Meanwhile, the paleosalinity of the watermasses also changed dramatically, showing fluctuation between fresh and brackish water conditions in the two sags. Furthermore, the relatively dry climate resulted in a low terrestrial influx and subsequent low input of nutrients, might have contributed to low paleo-productivity in photic zone (Fig. 11b). Such conditions were unfavorable for organic matter accumulation, which is reflected by low TOC values of K_2qn^{2+3} in both cores.

6. Conclusions

The role of Late Cretaceous marine incursions and their contribution to the formation of organic-rich shales within the Songliao Basin has been extensively studied. However, there was ambiguity regarding how these marine incursions affect the quality of source rocks across the lateral extent of the basin's Central Depression. High-resolution sedimentary features and geochemical assessments, including both elemental and Sr isotopic ratios have been analyzed between two drilled wells from the west (i.e., GY8HC Well from the Gulong Sag) and the east (i.e., ZY1 Well from the Sanzhao Sag) of the Central Depression. All the evidence suggests that marine incursions have a positive effect on the quality of K_2qn^1 source rocks in the Sanzhao Sag, which is probably due to the rising lake level and increasing salinity of the watermasses. In such scenarios, marine organisms might have contributed to an increase in organic matter and fostered an ideal environment for the preservation of organic matter through deposition. Compared with the Sanzhao Sag, the marine incursion events have less effect on the deposition of source rocks in the Gulong Sag. The lake exhibited characteristics of being fresh-brackish, possibly due to reduced seawater mixing. This study offers an extensive exploration into assessing the impact of the Late Cretaceous marine incursions on the Qingshankou source rocks within the Central Depression of the Songliao Basin.

CRediT authorship contribution statement

Ruiqian Chen: Writing – review & editing, Writing – original draft, Project administration, Methodology, Investigation, Funding acquisition, Data curation, Conceptualization. **Xin Bai:** Writing – review & editing, Software, Resources, Data curation. **Chengzheng Huang:** Visualization, Software. **Xia Wu:** Visualization. **Fei Shang:** Project administration, Funding acquisition.

Declaration of competing interest

The authors declare that they have no known competing financial interests or personal relationships that could have appeared to influence the work reported in this paper.

Data availability

Data will be made available on request.

Acknowledgements

We would like to thank the National Natural Science Foundation of China (Project No. 41702126) and PetroChina Science and Technology Project (No. KT2021-06-01) for their financial support. We really appreciate the editor Dr. Hui Tian and two reviewers Dr. Thomas Algeo and Dr. Katz for their detailed and constructive comments in improving the manuscript. We would also like to thank Daqing Oilfield Company for collecting core samples.

Appendix A. Supplementary data

Supplementary data to this article can be found online at https://doi.org/10.1016/j.marpetgeo.2024.107140.

References

Abshire, M., Romaniello, S., Kuzminov, A., Cofrancesco, J., Severmann, S., Riedinger, N., 2020. Uranium isotopes as a proxy for primary depositional redox conditions in organic-rich marine systems. Earth Planet Sci. Lett. 529, 115878.

Algeo, T., Lyons, T.W., 2006. Mo–total organic carbon covariation in modern anoxic marine environments: implications for analysis of paleoredox and paleohydrographic conditions. Paleoceanography 21, PA1016.

Algeo, T., Ingall, E., 2007. Sedimentary C_{org}:P ratios, paleocean ventilation, and Phanerozoic atmospheric pO_2. Palaeogeogr. Palaeoclimatol. Palaeoecol. 256, 130–155.

Algeo, T.J., Li, C., 2020. Redox classification and calibration of redox thresholds in sedimentary systems. Geochem. Cosmochim. Acta 287, 8–26.

Algeo, T.J., Liu, J., 2020. A re-assessment of elemental proxies for paleoredox analysis. Chem. Geol. 540, 119549.

Barrera, E., Johnson, C.C., 1999. Evolution of the cretaceous ocean – climate system. Geol. Soc. Amer. SP332 Boulder, Colorado 1–445.
Bosio, G., Malinverno, E., Collareta, A., Di Celma, C., Gioncada, A., Parente, M., Bianucci, G., 2020. Strontium isotope stratigraphy and the thermophilic fossil fauna from the middle miocene of the east pisco basin (Peru). J. S. Am. Earth Sci. 97, 102399.
Bwire Ojiambo, S., Berry Lyons, W., Welch, K., 2003. Strontium isotopes and rare earth elements as tracers of groundwater-lake water interactions, Lake Naivasha, Kenya. Appl. Geochem. 18, 1789–1805.
Cao, H., He, W., Chen, F., Kong, D., 2020. Superheavy pyrite in the Upper Cretaceous mudstone of the Songliao Basin, NE China and its implication for paleolimnological environments. J. Asian Earth Sci. 189, 104156.
Cao, H., He, W., Chen, F., Shan, X., Kong, D., Hou, Q., Pu, X., 2021. Integrated chemostratigraphy ($\delta^{13}C$-$\delta^{34}S$-$\delta^{15}N$) constrains Cretaceous lacustrine anoxic events triggered by marine sulfate input. Chem. Geol. 559, 119912.
Chen, R., Sharma, S., 2016. Role of alternating redox conditions in the formation of organic-rich interval in the middle devonian marcellus shale, appalachian basin, USA. Palaeogeogr. Palaeoclimatol. Palaeoecol. 446, 85–97.
Chen, R., Shang, F., Cao, Y., Song, L., Li, Z., 2022. A comparative study of oil shale deposition in the Upper Cretaceous Nenjiang Formation, NE China: evidence from petrographic and geochemical analyses. J. Petrol. Sci. Eng. 219, 111–130.
Feng, Z., Jia, C., Xie, X., Zhang, S., Feng, Z., Cross, T., 2010. Tectonostratigraphic units and stratigraphic sequences of the nonmarine Songliao basin, northeast China. Basin Res. 22, 79–95.
Feng, Z., Fang, W., Li, Z., Wang, X., Huo, Q., Huang, C., Zhang, J., Ceng, H., 2011. Depositional environment of terrestrial petroleum source rocks and geochemical indicators in the Songliao Basin. Sci. China Earth Sci. 54, 1304–1317.
Gao, R., Cai, X., 1997. Hydrocarbon Formation Conditions and Distribution Rules in the Songliao Basin. Petroleum Industry Press, Beijing (in Chinese).
Hou, D., Li, M., Huang, Q., 2000. Marine transgressional events in the gigantic freshwater lake Songliao: paleontological and geochemical evidence. Org. Geochem. 31, 763–768.
Hou, H., Shao, L., Li, Y., Liu, L., Liang, G., Zhang, W., Wang, W., 2022. Effect of paleoclimate and paleoenvironment on organic matter accumulation in lacustrine shale: constraints from lithofacies and element geochemistry in the northern Qaidam Basin, NW China. J. Petrol. Sci. Eng. 208, 109350.
Hu, J.F., Peng, P.A., Liu, M.Y., Xi, D.P., Song, J.Z., Wan, X.Q., Wang, C.S., 2015. Seawater incursion events in a cretaceous paleo-lake revealed by specific marine biological markers. Sci. Rep. 5, 9508.
Huang, F., Huang, Q., 1998. Rhythm of geological events and interaction of different geospheres in Mesozoic of Songliao Basin. Petrol. Explor. Dev. 5 (in Chinese with English Abstracts).
Huang, Y., Yang, G., Gu, J., Wang, P., Huang, Q., Feng, Z., Feng, L., 2013. Marine incursion events in the late cretaceous songliao basin: constraints from sulfur geochemistry records. Palaeogeogr. Palaeoclimatol. Palaeoecol. 385, 152–161.
Ingram, B., Depaolo, D., 1993. A 4300 year strontium isotope record of estuarine paleo-salinity in San Francisco Bay, California. Earth Planet Sci. Lett. 119, 103–119.
Jacobsen, S., Kaufman, A., 1991. The Sr, C and O isotopic evolution of Neoproterozoic seawater. Chem. Geol. 161, 37–57.
Jones, M., Ibarra, D., Gao, Y., Sageman, B., Selby, D., Chamberlain, C., Graham, S., 2018. Evaluating late cretaceous OAEs and the influence of marine incursions on organic carbon burial in an expansive East Asian paleo-lake. Earth Planet Sci. Lett. 484, 41–52.
Lafargue, E., Marquis, F., Pillot, D., 1998. Rock-eval 6 applications in hydrocarbon exploration, production, and soil contamination studies. Oil Gas Sci. Technol. 53, 421–437.
Lan, Z., Chen, Z., Li, X., Kaiho, K., 2013. Microbially induced sedimentary structures from the mesoproterozoic huangqikou formation, helan mountain region, northern China. Precambrian Res. 233, 73–92.
Li, D., Li, R., Zhu, Z., Xu, F., 2018. Elemental characteristics of lacustrine oil shale and its controlling factors of palaeo-sedimentary environment on oil yield: a case from Chang 7 oil layer of Triassic Yanchang Formation in southern Ordos Basin. Acta Geochimica 37, 228–243, 2018.
Li, L., Liu, Z., Sun, P., Li, Y., George, S., 2020. Sedimentary basin evolution, gravity flows, volcanism, and their impacts on the formation of the Lower Cretaceous oil shales in the Chaoyang Basin, northeastern China. Mar. Petrol. Geol. 119, 104472.
Liu, Y., Wang, H., Zhang, J., Liu, Z., Chen, F., Wang, X., Zhang, S., Liu, H., 2023. Rare earth elemental and Sr isotopic evidence for seawater intrusion event of the Songliao Basin 91 million years ago. Petrol. Sci. 20, 1347–1362.
Martinez-Ruiz, F., Kastner, M., Gallego-Torres, D., Rodrigo-Gámiz, M., Nieto-Moreno, V., Ortega-Huertas, M., 2015. Paleoclimate and paleoceanography over the past 20,000 yr in the Mediterranean Sea Basins as indicated by sediment elemental proxies. Quat. Sci. Rev. 107, 25–46.
McLennan, S., 1989. Rare earth elements in sedimentary rocks; influence of provenance and sedimentary processes. Rev. Mineral. Geochem. 21, 169–200.
McLennan, S., 2001. Relationships between the trace element composition of sedimentary rocks and upper continental crust. G-cubed 2 (4).
Palmer, M., Elderfield, H., 1985. Sr isotope composition of sea water over the past 75 Myr. Nature 314, 526–528.
Peng, J., 2022. What besides redox conditions? Impact of sea-level fluctuation on redox sensitive trace-element enrichment pattern in marine sediments. Svience China Earth Science 65, 1985–2004.
Peros, M., Reinhardt, E., Schwarcz, H., Davis, A., 2007. High-resolution paleo-salinity reconstruction from laguna de la leche, north coastal cuba, using Sr, O, and C isotopes. Palaeogeogr. Palaeoclimatol. Palaeoecol. 245, 535–550.
Reinhardt, E., Jean Stanley, D., Timothy Patterson, R., 1998. Strontium isotopic-paleontological method as a high-resolution paleo-salinity tool for lagoonal environments. Geology 26, 1003.
Sageman, B.B., Murphy, A.E., Werne, J.P., Ver Straeten, C.A., Hollander, D.J., Lyons, T. W., 2003. A tale of shales: the relative roles of production, decomposition, and dilution in the accumulation of organic-rich strata, Middle–Upper Devonian, Appalachian basin. Chem. Geol. 195, 229–273.
Sattouf, M., Kratz, S., Diemer, K., Rienitz, O., Fleckenstein, J., Schiel, D., Schnug, E., 2007. Identifying the origin of rock phosphates and phosphorus fertilizers through high precision measurement of the strontium isotopes ^{87}Sr and ^{86}Sr. Landbauforschung Völkenrode 57, 1–11.
Spivack, A., Palmer, M., Edmond, J., 1987. The sedimentary cycle of the boron isotopes. Geochem. Cosmochim. Acta 51, 1939–1949.
Sun, L., Cui, B., Zhu, R., Wang, R., Feng, Z., Li, H., Zhang, J., Gao, B., Wang, Q., Zeng, H., Liao, Y., Jiang, H., 2023. Shale oil enrichment evaluation and production law in Gulong Sag, Songliao Basin, NE China. Petrol. Explor. Dev. 50, 441–454.
Tribovillard, N., Algeo, T., Lyons, T., Ri boulleau, A., 2006. Trace metals as paleoredox and paleoproductivity proxies: an update. Chem. Geol. 232, 12–32.
Tribovillard, N., Algeo, T.J., Baudin, F., Riboulleau, A., 2012. Analysis of marine environmental conditions based onmolybdenum–uranium covariation—applications to Mesozoic paleoceanography. Chem. Geol. 324–325, 46–58.
Wang, C., Gao, Y., Wang, P., Wu, H., Lü, Q., Zhu, Y., Wan, X., Zou, C., Huang, Y., Gao, Y., Xi, D., Wang, W., He, H., Feng, Z., Yang, G., Deng, C., Zhang, L., Wang, T., Hu, B., Cui, L., Peng, C., Yu, E., Huang, H., Yang, L., Wu, Z., 2024. International continental scientific drilling project of the songliao basin: terrestrial geological records of the cretaceous dinosaur age. Earth Sci. Front. 31, 511–534.
Wang, P., Huang, Y., Wang, C., Feng, Z., Huang, Q., 2013a. Pyrite morphology in the first member of the late Cretaceous Qingshankou Formation, Songliao basin, northeast China. Palaeogeogr. Palaeoclimatol. Palaeoecol. 385, 125–136.
Wang, C., Scott, R., Wan, X., Graham, S., Huang, Y., Wang, P., Wu, H., Dean, W., Zhang, L., 2013b. Late cretaceous climate changes recorded in Eastern Asian lacustrine deposits and North American Epieric sea strata. Earth Sci. Rev. 126, 275–299.
Wang, L., Lv, D., Hower, J.C., Zhang, Z., Raji, M., Tang, J., Liu, Y., Gao, J., 2022. Geochemical characteristics and paleoclimate implication of middle jurassic coal in the Ordos Basin, China. Ore Geol. Rev. 144, 104848.
Wang, P., Mattern, F., Didenko, N., Zhu, D., Singer, B., Sun, X., 2016. Tectonics and cycle system of the Cretaceous Songliao Basin: an inverted active continental margin basin. Earth Sci. Rev. 159, 82–102.
Wedepohl, K., 1991. The composition of the upper earth's crust and the natural cycles of selected metals. Metal in natural raw materials, natural resources. Metals and their compounds in the environment. Occurrence, Analysis and Biological Relevance, pp. 3–17.
Wei, W., Algeo, T.J., Lu, Y., Lu, Y.C., Liu, H., Zhang, S., Peng, L., Zhang, J., Chen, L., 2018. Identifying marine incursions into the paleogene bohai bay basin lake system in northeastern China. Int. J. Coal Geol. 200, 1–17.
Wei, W., Algeo, T., 2020. Elemental proxies for paleo-salinity analysis of ancient shales and mudrocks. Geochem. Cosmochim. Acta 287, 341–366.
Wen, H., Zheng, R., Qing, H., 2007. Characteristics of strontium isotopic geochemistry of Sub-lacustrine hydrothermal sedimentary rock of Xiagou For- mation in Qingxi Sag, Jiuquan Basin. Acta Sedimentalogica Sinica 27, 642–649.
Werne, J., Sageman, B., Lyons, T., Hollander, D., 2002. An integrated assessment of a "type euxinic" deposit: evidence for multiple controls on black shale deposition in the Middle Devonian Oatka Creek Formation. Am. J. Sci. 302, 110–143.
Wu, H., Feng, C., Kang, X., Fu, D., Feng, J., Zhang, Y., Zhou, J., Hu, T., 2023. Positive and negative effects of marine transgression on the quality of lacustrine source rocks in the Upper Cretaceous Songliao Basin, China. Mar. Petrol. Geol. 153, 106267.
Xi, D., Wan, X., Feng, Z., Li, S., Feng, Z., Jia, J., Jin, X., Si, W., 2011. Discovery of Late Cretaceous foraminifera in the Songliao Basin: evidence from SK-1 and implications for identifying seawater incursions. Chin. Sci. Bull. 55, 3433–3436 (in Chinese with English abstract).
Xia, L., Cao, J., Hu, S., Li, S., 2019. How marine incursion influences the quality of lacustrine source rocks: the Paleogene Nanxiang Basin, eastern China. AAPG (Am. Assoc. Pet. Geol.) Bull. 103, 1071–1096.
Xu, B., Diao, H., Wang, N., He, J., Shi, J., Hu, B., Zhou, X., 2022. Geochemical characteristics and indicative significance of trace elements in the paleocene in Lishui sag, east China sea basin. Marine Geology Frontiers 38, 64–74 (In Chinese with English Abstract).
Xu, J., Bechtel, A., Sachsenhofer, R., Liu, Z., Gratzer, R., Meng, Q., Song, Y., 2015. High resolution geochemical analysis of organic matter accumulation in the Qingshankou Formation, upper cretaceous, Songliao Basin (NE China). Int. J. Coal Geol. 141, 23–32.
Yang, W., Gao, R., Guo, Q., Liu, S., 1985. Generation, Migration and accumulation of terrestrial oil in the Songliao Basin. Heilongjiang Scientific and Technological. Press, Harbin, pp. 50–158 (In Chinese with English Abstract).
Zhao, W., Wang, H., Yuan, X., Wang, Z., Zhu, G., 2010. Petroleum systems of Chinese nonmarine basins. Basin Res. 22, 4–16.
Zhu, R., Cui, J., Luo, Z., Li, S., Mao, Z., Su, L., 2020. The discussion on the genesis of carbonate concretions in Chang7 member of middle-upper Triassic Yanchang Formation of Ordos Basin. Acta Geol. Sin. 94, 1–13.
Zhu, X., Cao, J., Xia, L., Bian, L., Liu, J., Zhang, R., 2023. Links between marine incursions, lacustrine anoxia and organic matter enrichment in the Upper Cretaceous Qingshankou Formation, Songliao Basin, China. Mar. Petrol. Geol. 158, 106536.
Zou, C., Zhu, R., Chen, Z., Ogg, J., Wu, S., Dong, D., Yang, Z., 2019. Organic-matter-rich shales of China. Earth Sci. Rev. 189, 51–78.